land

MDPI

Article

Nonlinear Effects of Human Settlements on Seasonal Land Surface Temperature Variations at the Block Scale: A Case Study of the Central Urban Area of Chengdu

Muze Zhang [1], Tong Hou [1], Yuping Ma [1], Mindong Liang [1], Jiayu Yang [1], Fengshuo Sun [1] and Enxu Wang [1,2,*]

[1] Jangho Architecture College, Northeastern University, Shenyang 110169, China; 20207842@stu.neu.edu.cn (M.Z.); 20207832@stu.neu.edu.cn (T.H.); 20207864@stu.neu.edu.cn (Y.M.); 20207805@stu.neu.edu.cn (M.L.); 20217636@stu.neu.edu.cn (J.Y.); 20217673@stu.neu.edu.cn (F.S.)
[2] Liaoning Key Laboratory of Urban and Architectural Digital Technology, Shenyang 110169, China
* Correspondence: wangenxu@mail.neu.edu.cn

Abstract: The land surface temperature (LST) in the central urban area has shown a consistent upward trend over the years, exacerbating the surface urban heat island (SUHI) effect. Therefore, this study focuses on the central urban area of Chengdu, using blocks as the research scale. The Gradient Boosting Decision Tree (GBDT) model and SHAP values are employed to explore the nonlinear effects of human settlements (HS) on LST across different seasons. The results show that (1) At the block scale, the overall impact of HS on LST across all four seasons tracks the following order: built environment (BE) > landscape pattern (LP) > socio-economic development (SED). (2) LP is the most important factor affecting LST in summer, while the BE has the greatest influence on LST during spring, autumn, and winter. (3) Most HS indicators exhibit seasonal variations in their impact on LST. The impervious surface area (ISA) exhibits a significant positive impact on LST during spring, summer, and autumn. In contrast, the nighttime light index (NTL) and functional mix degree (FMD) exert a significant negative influence on LST in spring, autumn, and winter. Additionally, the normalized difference vegetation index (NDVI) negatively affects LST in both spring and summer. Moreover, connectivity (CNT) and functional density (FPD) demonstrate notable threshold effects in their influence on LST. (4) Certain HS indicators exhibit interaction effects, and some combinations of these indicators can effectively reduce LST. This study reveals HS–LST interactions through multidimensional analysis, offering block-scale seasonal planning strategies for sustainable urban thermal optimization.

Keywords: block scale; central urban area; gradient boosting decision tree; human settlements; land surface temperature; seasonal variation

check for updates

Academic Editor: Marko Scholze

Received: 18 February 2025
Revised: 20 March 2025
Accepted: 21 March 2025
Published: 25 March 2025

Citation: Zhang, M.; Hou, T.; Ma, Y.; Liang, M.; Yang, J.; Sun, F.; Wang, E. Nonlinear Effects of Human Settlements on Seasonal Land Surface Temperature Variations at the Block Scale: A Case Study of the Central Urban Area of Chengdu. *Land* **2025**, *14*, 693. https://doi.org/10.3390/land14040693

Copyright: © 2025 by the authors. Licensee MDPI, Basel, Switzerland. This article is an open access article distributed under the terms and conditions of the Creative Commons Attribution (CC BY) license (https://creativecommons.org/licenses/by/4.0/).

1. Introduction

In the process of urbanization, cities worldwide are increasingly facing severe climate challenges, among which the urban heat island (UHI) effect is one of the most pressing issues. The UHI effect is defined as the significant temperature difference between urban areas and their surrounding rural regions [1]. Chinese cities, especially large cities like Chengdu, are experiencing an increasingly severe heat island effect, posing significant challenges to the sustainable development of urban areas [2]. UHI intensifies, reaching its peak during summer, severely impacting urban residents' thermal comfort and health [3,4]. The detrimental effects of UHI are multifaceted, including the accumulation of air pollution, changes in vegetation phenology, and instability in water supply [5]. The UHI effect is

commonly referred to as the canopy urban heat island (CUHI), which is primarily estimated using in situ observational data [6,7]. In contrast, the surface urban heat island (SUHI) is derived from thermal infrared remote sensing imagery [8]. The difference in LST between urban and rural areas is defined as SUHI [9]. Consequently, remote sensing technology has provided a new perspective for large-scale UHI studies. Due to its advantages in rapid satellite image acquisition, extensive spatial coverage, and cost efficiency, research on SUHI has gained increasing attention in recent years.

In recent years, scholars have extensively studied the SUHI effect using tools such as remote sensing technology and geographic information systems (GIS). By analyzing the relationship between urban spatial morphology factors and LST, researchers have explored the impact of the built environment on the SUHI effect [10–12]. Among these, two-dimensional morphological parameters such as building coverage and impervious surface area have been identified as the most influential factors [13,14]. Further research has evaluated the impact of urban surface configurations on LST, exploring how landscape metrics influence LST [15]. Additionally, studies have discussed the role of quantified landscape pattern indices. For instance, in cities like Wuhan, China, scholars introduced the spatial connectivity index to quantify the influence of landscape patterns on LST, finding a significant negative correlation between the connectivity index and LST [16]. In studies on the impact of socioeconomic development on LST, it has been found that indicators such as population density and the nighttime light index also have a significant influence on LST [17,18]. However, few studies have explored the influencing factors of LST from a comprehensive perspective that includes the built environment, landscape pattern, and socioeconomic development [19–21]. These three aspects are essential for evaluating human settlements in central urban areas, the primary spaces for human habitation and production. Together, they comprehensively reflect the core content system influencing LST in current research [22,23]. Based on this, this study aims to select human settlement indicators from the built environment (BE), landscape pattern (LP), and socioeconomic development (SED) to explore the nonlinear impact of HS on LST, thereby providing theoretical insights for reducing LST. In selecting the independent variables, drawing on the previous research and focusing on our research objective—the impact of HS on LST—this study first selected independent variables from the BE and LP aspects. Initially, the significant impact of green spaces and water bodies on LST has been well-documented [17,24,25]. However, due to the extreme scarcity of water bodies in Chengdu's central urban area, this study used only the normalized difference vegetation index (NDVI) to represent the level of greening. The two-dimensional and three-dimensional characteristics of the built environment also have a significant impact on the urban thermal environment [10,14]. Two-dimensional composition indicators, such as building coverage ratio (BCR) and impervious surface area (ISA), are used to represent specific land use or cover types in urban areas [13,14,24]. Two-dimensional configuration indicators, such as patch density (PD) and connectivity (CNT), are used to describe how cover types are distributed and arranged [24,25]. Additionally, three-dimensional features, such as mean building height (MH), are incorporated [13,24]. Additionally, this study selected more indicators related to landscape patterns, such as the landscape division index (LDI), the contagion index (CTG), and the Shannon diversity index (SHDI) [18], to better characterize the impact of the distribution and arrangement of urban land cover types on LST. Similar landscape pattern indices are effective in reflecting how landscapes promote or hinder ecological flows and are widely used in the field of landscape ecology [26]. By utilizing these indices to represent land use patterns, this study can explore how to reduce the connectivity of heat landscapes to mitigate SUHI. Subsequently, this study also selected economic and functional factors such as road density (RD), functional density (FPD), and population density (POD), which have been proven to

affect LST [17]. In constructing the HS indicator system, this study further included the functional mixing degree (FMD) to explore the impact of land use functions within the area, along with the nighttime light index (NTL), which reflects socioeconomic attributes [18].

Additionally, the seasonal variation in the UHI effect has garnered attention from researchers [27]. One seasonal UHI analysis showed that the surface UHI effect in Hefei exhibits significant differences across seasons and local climate zones, with the most pronounced UHI observed in summer [17]. The synergistic effect of UHI and heatwaves also requires attention. A study conducted in Guangzhou found that during summer heatwaves, the UHI effect significantly intensified in densely built urban areas [28]. Similarly, scholars have investigated the formation mechanisms and seasonal variations in SUHI at local, regional, and global scales [17,29]. For example, in studies on the seasonal variations of SUHI, MODIS LST data have been widely used [30]. The application of this remote sensing product facilitates land surface retrieval based on LST, enabling the quantification in SUHI intensity and the exploration of its seasonal variation mechanisms [6,31]. Moreover, most scholars focus on the entire city as the study area, paying less attention to the more complex thermal environment issues of central urban areas. In terms of research scale, most studies use a grid-based scale to comprehensively examine the impact of 2D/3D built environment indicators on LST [32,33]. However, urban morphology, particularly buildings, road networks, and open spaces, is often segmented into discrete parts by grids and buffers [34,35]. The studies investigating the relationship between fragmented urban morphology and LST fail to provide intuitive references for mitigating the UHI effect. Based on this, this study takes the central urban area of Chengdu, a typical large city in western China, as the study area, using urban blocks as the research unit to investigate the nonlinear impact of the built environment on LST. A block refers to an urban land unit enclosed by roads, serving as the basic unit for urban design differentiation, with the aim of shaping urban morphology and improving the urban thermal environment [18,36]. Due to this unique partitioning method, there are significant size variations among blocks, and the typical block size varies depending on the classification criteria. However, each block serves as the fundamental unit for calculating HS indicators and analyzing their relationship with LST.

With the continuous development of satellite remote sensing technology, different remote sensing images, such as Landsat and MODIS, can rapidly reflect the differences in urban surface temperatures, providing a foundation for microclimate research [37,38]. Additionally, the application of the Google Earth Engine (GEE) platform offers opportunities for the geometric and radiometric correction of large-scale satellite images, facilitating the analysis of the urban thermal environment [39]. This enables faster processing and more accurate results. This study comprehensively applies machine learning algorithms, including Gradient Boosting Decision Tree (GBDT) and interpretable machine learning methods such as SHAP, to analyze and predict LST in the central urban area. Linear regression methods have typically been used to model the relationship between LST and built environment attributes [24,40,41]. At the same time, many studies analyzing the urban thermal environment based on LST and UHI have employed machine learning techniques, demonstrating the prevalence of nonlinear relationships in related research [42–44]. For instance, methods such as random forest (RF) and extreme gradient boosting (XGBoost) have been widely applied in related research [20,45]. The advantage of these nonlinear models lies in their lack of assumption regarding any predefined relationships, allowing them to capture complex nonlinear associations, particularly when the relationships between independent variables vary over time or under different conditions. For instance, when addressing the complex interactions between urban morphology and LST, nonlinear models have demonstrated high efficiency [46]. Among them, the GBDT model is particularly effective in addressing

multicollinearity issues, and it is capable of handling missing and outlier values. Therefore, this study selects GBDT for its ability to handle a wide range of parameters. However, research on the nonlinear impact of the built environment on LST remains insufficiently comprehensive [18]. This is due to the fact that urban planning typically requires a holistic consideration of multiple environmental factors, while existing studies have largely focused on analyzing the impact of individual factors on LST, neglecting the interactions between different elements and their potential influence on LST. Therefore, employing machine learning techniques such as GBDT to investigate the nonlinear relationships between urban environmental indicators and LST not only helps identify the relative importance of each indicator and its nonlinear influence on LST but also enhances model interpretability and reliability through the SHAP (SHapley Additive exPlanations) method at both global and local levels. This approach further facilitates the analysis of interactive effects among different indicators on LST.

The specific objectives of this study are (1) to analyze the nonlinear relationships and interactions between different human settlement indicators and LST using GBDT and SHAP; (2) to classify human settlement indicators based on their varying degrees of influence and explore the effects of research scale; (3) to investigate the seasonal variations in the mechanisms through which human settlement indicators influence LST; (4) to compare study data and provide effective recommendations and climate adaptation strategies for improving the urban thermal environment. Through this research, we aim to offer new ideas and strategies for improving the complex thermal environment of central urban areas in Chengdu and other similar cities in China, ultimately creating a healthy and comfortable urban living environment. The findings of this study will contribute to achieving this goal.

2. Materials

2.1. Study Area

Chengdu is located in the western part of the Sichuan Basin and is a major megacity in southwestern China. It has an expansive built-up area of 949.6 square km, with a permanent population of 21.403 million and an urbanization rate as high as 80.5% (Data source: http://cdstats.chengdu.gov.cn/). This intense urbanization, coupled with rapid socio-economic development, has resulted in significant environmental and climatic challenges, particularly urban heatwaves [47]. During the summer daytime in Chengdu, the expansion of the urban heat island area has led to the merging of Chengdu and its neighboring satellite towns into a unified heat island region [48]. Due to the basin topography and stagnant meteorological conditions in the central research area of the Chengdu Plain, the average wind speed is only 0.7 m/s, with over 240 days of calm each year [49,50], and it is classified as a subtropical monsoon climate zone [51]. The meteorological characteristics of high temperature, high humidity, and calm winds exacerbate the UHI effect and the thermal stress experienced by urban residents.

In selecting the research area, this study combined the administrative divisions and geographical boundaries of Chengdu, choosing the “central five districts” within the Fourth Ring Road as the study area. Administratively, Jinjiang District, Qingyang District, Jinniu District, Wuhou District, and Chenghua District form the five major administrative regions of Chengdu’s central urban area, collectively known as the “central five districts”, with a total area of 473.63 square km. This area constitutes the core of Chengdu. Therefore, our research area represents the typical central urban area of Chengdu, where overall LST is highest, and the UHI effect is most pronounced. This study integrated previous block division standards, forming blocks through the enclosure of secondary and tertiary roads, resulting in a total of 2399 blocks, as shown in Figure 1. The average area of the final blocks

is 0.171584 square km, with the maximum and minimum areas being 6.975864 square km and 0.002126 square km, respectively.

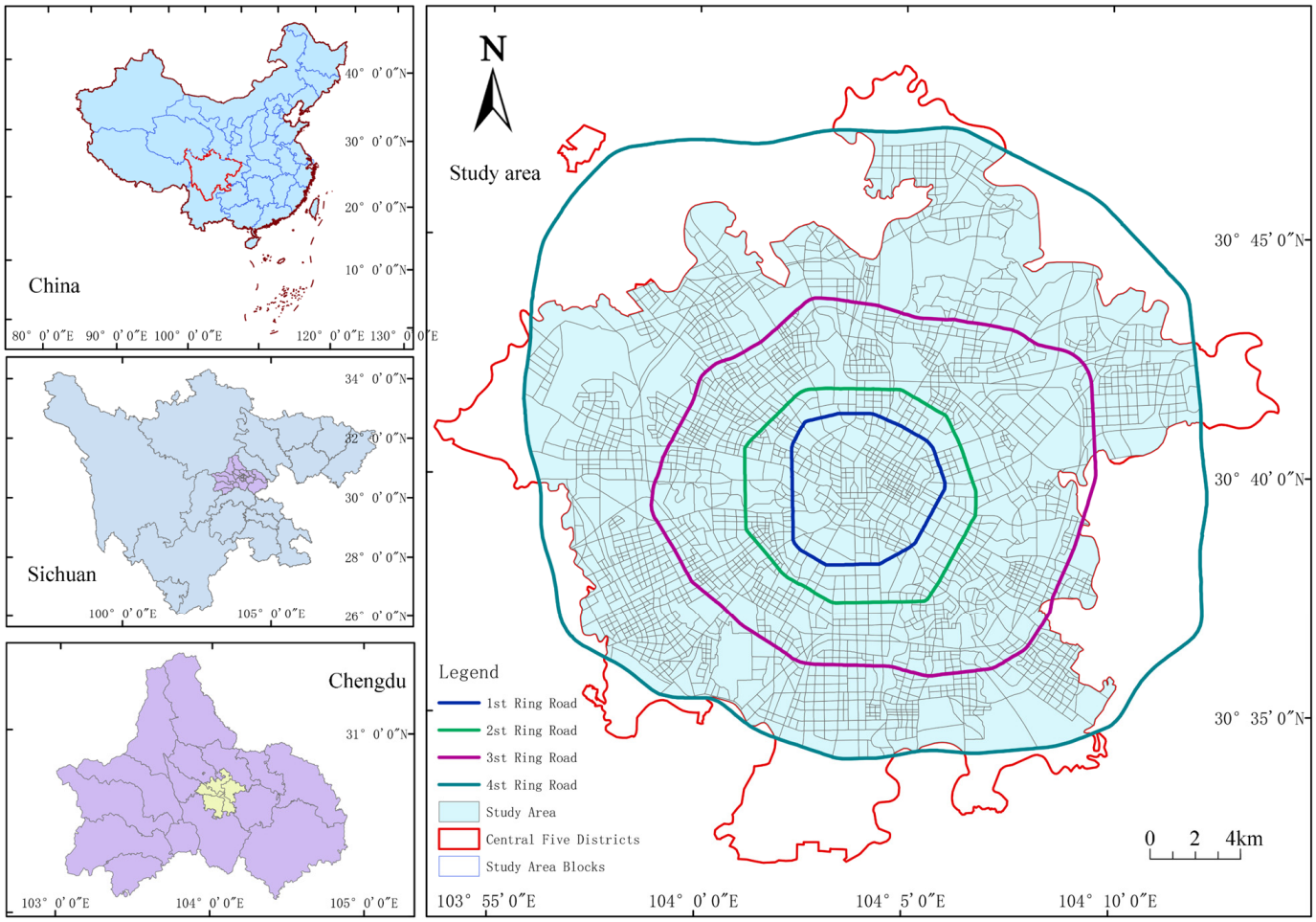

Figure 1. Location of Chengdu central urban area.

2.2. The Establishment of the Indicator System

In this study, we established a variable system (Table 1) consisting of the dependent variable (LST) and independent variables (HS indicators). The HS is a comprehensive concept encompassing multiple factors such as natural, social, and economic aspects. It focuses on studying the interrelationships between the forms of human settlements and the environment. The central area of Chengdu, as an extremely large human settlement, involves complex elements of the human settlement environment and their interaction relationships. Therefore, this study established the HS indicator system. The BE indicators include BCR, RD, ISA, MH, and NDVI. The LP indicators include CTG, SHDI, PD, LDI, and CNT. The SED indicators include POD, FPD, NTL, and FMD, as shown in Table 1.

Table 1. Human settlements index.

Dimensions	Indicator Factor	Abbr.	Description	Spatial Resolution
Socio-economic development	Population density	POD	Population density per unit area	100 m
	Functional density	FPD	Average number of POIs per thousand people	Vector data
	Nighttime light index	NTL	Nighttime light brightness index	100 m
	Mixed functionality degree	FMD	Average POI functional mixing degree across sixteen categories (e.g., business, culture)	Vector data

Table 1. *Cont.*

Dimensions	Indicator Factor	Abbr.	Description	Spatial Resolution
Built Environment	Building coverage ratio	BCR	Ratio of the total building footprint area to the land area occupied	Vector data
	Road density	RD	Ratio of total road network length to the land area served	Vector data
	Impermeable surface ratio	ISA	Proportion of land covered by impervious surfaces (e.g., concrete and asphalt)	30 m
	Mean building height	MH	Average building height within the area	Vector data
	Normalized difference vegetation index	NDVI	Remote sensing index measuring vegetation coverage and health	30 m
Landscape pattern	Contagion index	CTG	Index measuring the aggregation or extension trend of different patch types	30 m
	Shannon diversity index	SHDI	Index measuring the richness and evenness of patch types in a landscape	30 m
	Patch density	PD	Number of different landscape patches per unit area	30 m
	Landscape division index	LDI	Index measuring the degree of landscape fragmentation	30 m
	Connectance index	CNT	Index measuring the interaction between different landscape patches	30 m

2.3. Data Collection

This study used Google Earth Engine (GEE, https://earthengine.google.com/) and Landsat 8 satellite imagery to calculate the LST of Chengdu. World Pop population data were extracted using ArcGIS tools (https://hub.worldpop.org/) to calculate population density at the block level, which was further adjusted using data from China's Seventh National Census. NDVI data were obtained through the National Science and Technology Resource Sharing Service Platform of China (http://www.nesdc.org.cn/). Different levels of road data were used to calculate road density, with the raw data sourced from OpenStreetMap (https://www.openstreetmap.org). The road data in this study were also sourced from OpenStreetMap, supplemented by Gaode Map, with ArcGIS 10.8 software used to construct the road network and manually divide the blocks. When calculating the two-dimensional and three-dimensional attributes of the city, this study obtained vector data such as building outlines from the Gaode platform (https://ditu.gaode.com/). The average height and building coverage ratio were calculated using ArcGIS tools. The POI data this study used also came from this platform. This study used the average number of POIs per thousand people to represent functional density. For the calculation of the functional mixing degree, this study applied the Shannon entropy theory. In this study, Gaode Map POIs were classified into sixteen major categories, covering functions such as business, culture, dining, sports, healthcare, and transportation. The results indicate that the average functional mixing degree in the study area is 0.695612. Landscape pattern indices such as the landscape division index were calculated using land use data obtained from the Digital Earth Open Platform (https://open.geovisearth.com/service/resource/31) by importing the data into the Fragstats 4.2 tool. This study calculated aggregation indices such as landscape division, patch density, and connectivity, as well as diversity indices such as the contagion index and the Shannon diversity index. The impervious surface area ratio was also calculated from the land use data. This study used the Luojia-1 satellite to obtain nighttime light images for the study area (http://59.175.109.173:8888/app/login.html) and calculated the nighttime light index as shown in Table 1 and Figure 2.

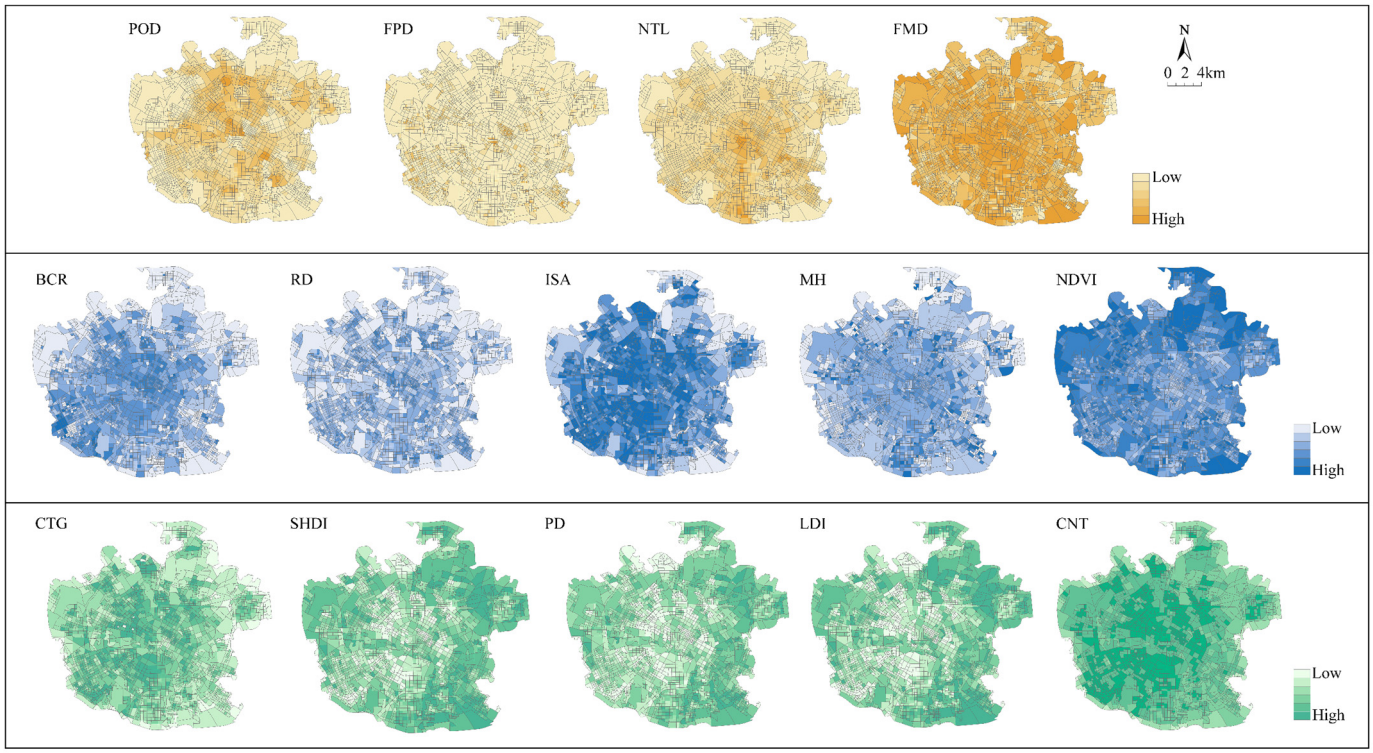

Figure 2. The level of HS indicators.

The selected study area, Chengdu, is situated in a basin with distinct climatic characteristics, but frequent cloudy weather poses a challenge [52]. Over the past five years, there have been very few clear, cloud-free images available for analysis. Therefore, it is necessary to select the most representative and high-quality images from the limited available data. When selecting weather and date data, ensuring reliable data for each season is key. The primary reference is the document on China's seasonal climate division (Climate Seasonal Division, cma.gov.cn) and the meteorological division method (spring is from March to May, summer from June to August, autumn from September to November, and winter from December to February). After filtering, the following four dates were selected based on high image quality, representing the typical characteristics of each season of Chengdu in Table 2. Additionally, the acquisition times were in close proximity, excluding nighttime data.

Table 2. LST seasonal date selection.

Date	Temperature	Weather	Cloudiness	Beijing Time
16 April 2023	19–34 °C	Cloudy to Clear	0.06%	11:32
05 July 2023	22–35 °C	Cloudy to Clear	0.23%	11:33
26 January 2023	8–22 °C	Cloudy to Clear	0.15%	11:33
05 February 2021	6–18 °C	Clear	0.42%	11:33

3. Methods

3.1. Google Earth Engine (GEE) Method for Calculating LST

GEE is a cloud computing application programming interface (API) that provides a fast and efficient cloud computing environment using open-source satellite imagery [53,54]. It also offers the opportunity to use large-scale satellite imagery that has undertaken geometric and radiometric correction. This study retrieved LST based on GEE. Based on the advantages of GEE, this study used the platform to obtain Landsat 8 OLI images with cloud cover of less than 5% for four dates in Chengdu. The acquired images were processed

directly on the GEE platform for cloud removal, atmospheric correction, radiometric correction, and mosaicking. Using the single-window algorithm, an LST inversion code was written on the GEE platform, and the thermal infrared band (Band 10) of Landsat 8 was used to retrieve the LST of Chengdu, as shown in Figure 3.

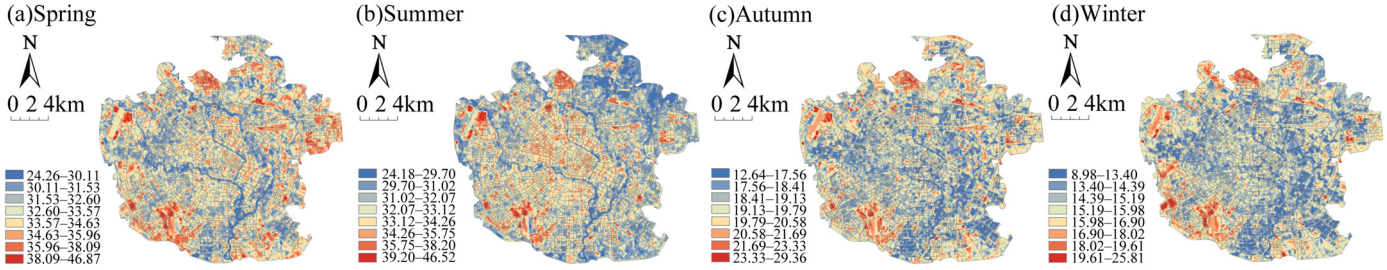

Figure 3. Seasonal changes in LST in Chengdu.

3.2. Gradient Boosting Decision Tree (GBDT) Model

The Gradient Boosting Decision Tree (GBDT) is well-suited for addressing issues with concentrated data feature distributions, and its accuracy surpasses that of algorithms like support vector machines and random forests. Additionally, for non-enterprise-level small sample data, its prediction accuracy is slightly higher than that of extreme gradient boosting (XGBoost), which prioritizes algorithm efficiency. Moreover, the ensemble boosting method is effective even with relatively small sample sizes [55].

The GBDT model can also generate partial dependence plots (PDPs), which visualize the marginal effects of features on prediction outcomes. In this study, we used the scikit-learn package in Python (version 1.3.2). After constructing the initial model, we utilized the GridSearchCV algorithm to fine-tune the hyperparameters. Due to computational constraints that prevented covering all possible parameter values, we supplemented GridSearchCV with the BayesSearchCV algorithm. This stochastic optimization algorithm employs Bayesian optimization to identify optimal hyperparameters over a broader range, creating an optimal model based on the current dataset for subsequent use. This study assesses the predictive accuracy and error of each model by calculating the coefficient of determination (R^2). R^2 is a statistical metric that quantifies the proportion of variance in the dependent variable that can be explained by the independent variables. Its value ranges from 0 to 1, with higher values indicating a better model fit and stronger explanatory power regarding data variability. For the different datasets corresponding to each season, the optimal set of hyperparameters for that specific season was determined, ensuring that the R-squared values of the optimal model on the test sets were all above 0.57.

3.3. SHapley Additive exPlanations (SHAP) Method

SHAP is a model interpretation package developed on the Python platform, based on the Shapley value concept from the cooperative game theory [56]. It can be used to interpret the outputs of machine learning models, which typically lack the interpretability of linear models. This is due to the "black box problem" in machine learning, where it is difficult to interpret the underlying reasons behind the prediction results. The advantage of SHAP lies in its ability to explain and visually represent the contribution of individual variables to the model's predictions, as well as the interaction effects between variables. SHAP interaction values, in particular, quantify the average contribution of each feature to the model's prediction under different feature combinations, thereby elucidating the interactions between features. This is crucial for understanding the impact of environmental factor interactions on UHR [57]. This study used the **shap** package in the Python environment to perform SHAP analysis, obtaining a total of 728 SHAP interaction values

plots. From these, this study selected 16 plots with significant interaction effects for further analysis.

3.4. Research System Framework

In this study, we established a variable system consisting of the dependent variable (LST) and independent variables (HS indicators), as shown in Table 1. HS is a comprehensive concept that encompasses various factors such as natural, social, and economic elements, focusing on the relationship between human settlement patterns and the environment. Given that the central urban area of Chengdu is a large-scale human settlement, involving complex human settlement factors and their interactions, we developed a HS indicator system comprising three aspects: BE, LP, and SED. The GBDT model and SHAP values are employed to explore the nonlinear effects of HS on LST across different seasons (Figure 4).

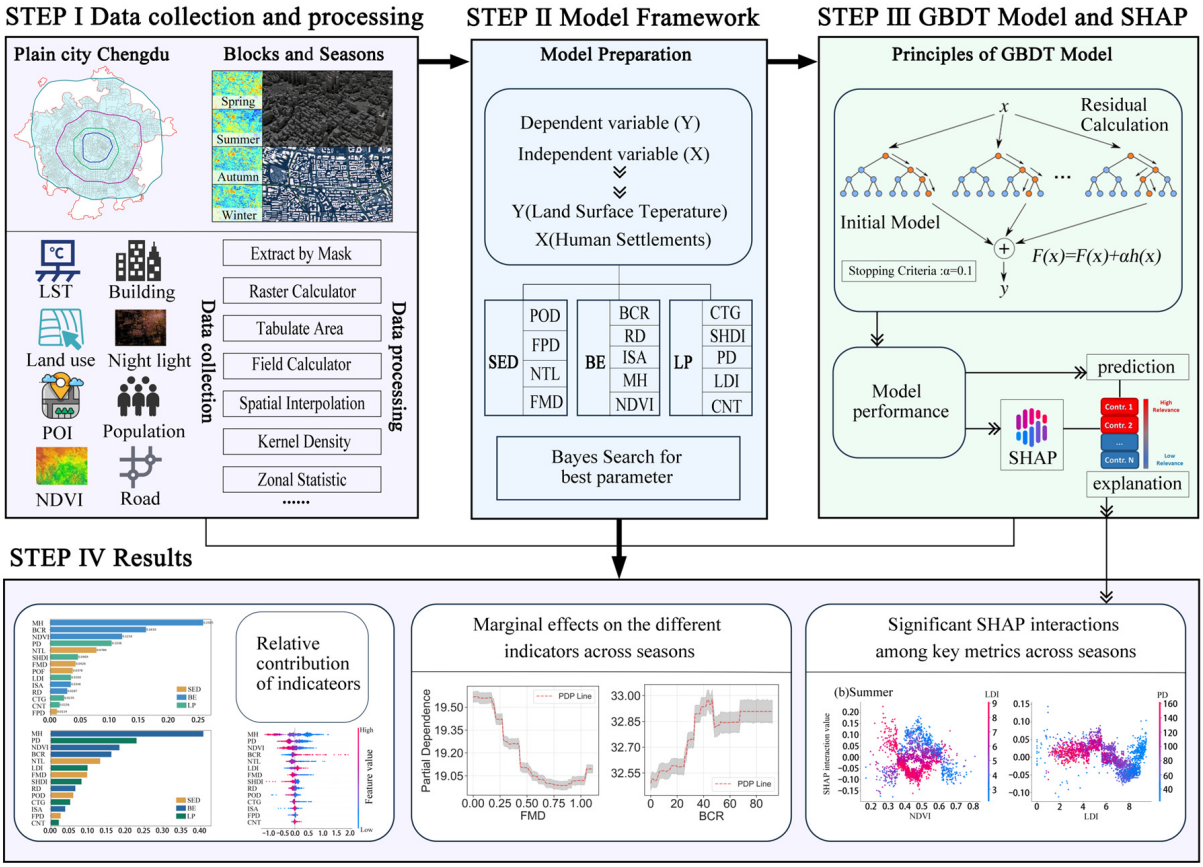

Figure 4. Research framework.

4. Results

4.1. Spatial Distribution of LST in Different Seasons Under Block Division

In spring, as temperatures recover from winter, the LST rises. The overall temperature within the city remains relatively high but is evenly distributed, with no pronounced hotspots. During summer, Chengdu experiences its highest temperatures, with an average LST of approximately 33 °C. The city center and high-density building areas are particularly hot, exhibiting a strong SUHI effect, likely due to heat retention and poor air circulation. Notably, Jinjiang and Wuhou districts, characterized by commercial hubs and high floor area ratios, experience significant temperature increases. In autumn, solar radiation weakens, leading to a gradual temperature decline. Qingyang District shows a relatively uniform temperature distribution, with the central area slightly cooler than the western and southern

parts. Although the SUHI effect persists, it is less pronounced than in summer. In winter, Chengdu experiences frequent rainfall and overcast conditions, with a maximum LST of only 21 °C. Jinjiang District and the city center maintain relatively higher temperatures, and the heat retention effect in urban built-up areas becomes more evident compared to autumn (Figure 5).

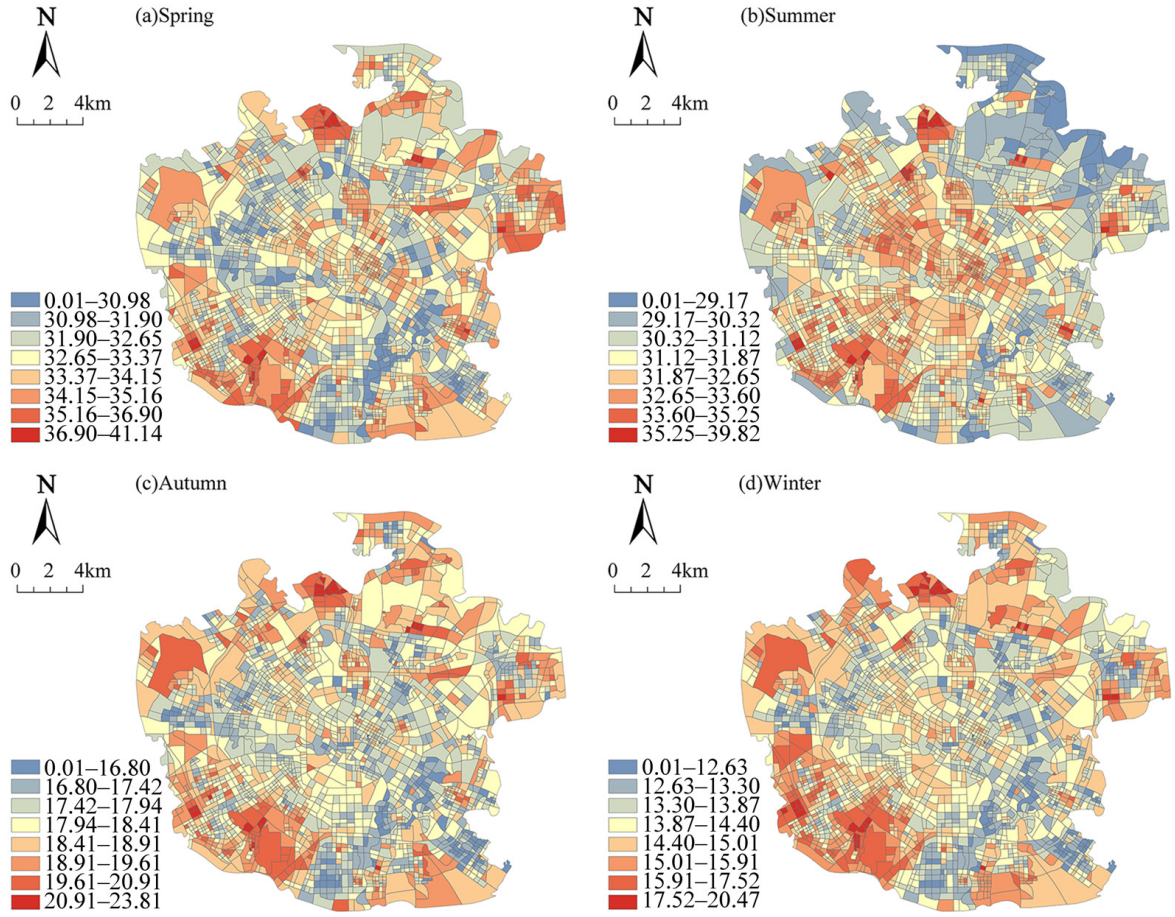

Figure 5. Seasonal changes in LST in Chengdu under block division.

4.2. The Relative Importance of HS Indicators on LST Impact

This study, based on the results of the trained models, employed relative feature importance and SHAP analysis methods to evaluate the relative importance of the HS index in influencing surface temperature across the spring, summer, autumn, and winter seasons in the central urban area of Chengdu.

Furthermore, this study provides a detailed analysis of the varying impact intensities of each indicator on surface temperature across different seasons. Relative feature importance was assessed by sequentially substituting each feature and observing the degree of impact on model performance, thereby evaluating the global contribution of each feature. SHAP analysis takes a local perspective for each sample, calculating the global contribution and directional influence of each feature on the target variable. The mean SHAP value reflects the overall impact of the feature, while each individual point represents the specific contribution of that feature in a particular sample. The results indicate that the ranking of important features derived from different methods is nearly identical, thereby enhancing the reliability of the findings in Figure 6.

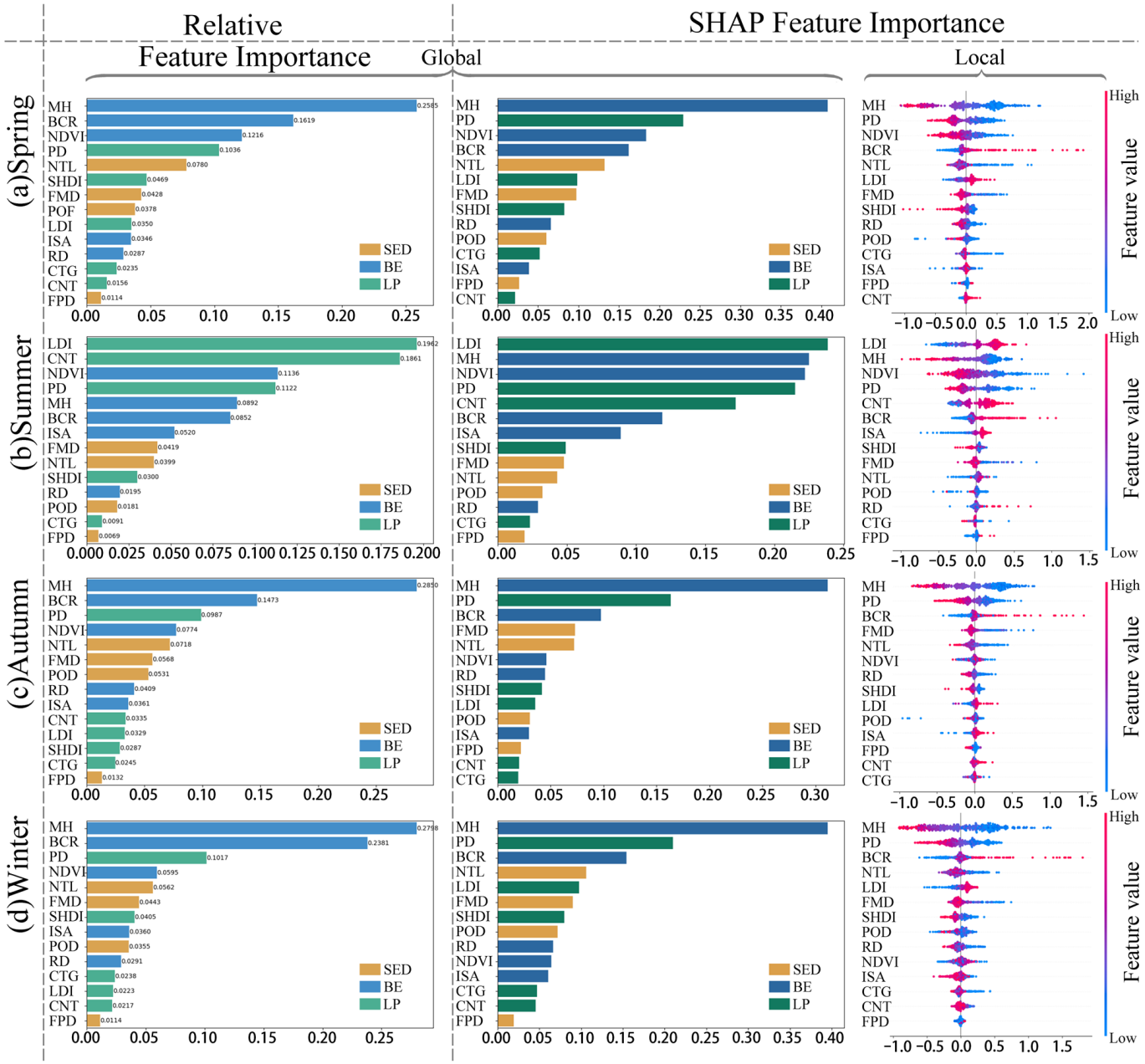

Figure 6. Relative and SHAP importance of LST in different seasons.

From the perspective of the different dimensions of HS, the overall seasonal impact on LST, from smallest to largest, takes the following order: built environment (BE) > landscape pattern (LP) > socio-economic development (SED). BE has the strongest influence on LST during spring, autumn, and winter, while LP has the greatest impact on LST during summer. It was notably observed that during the summer, the feature points of LDI, PD, and CND in the LP region were predominantly distributed in the positive zone, exerting a significant impact on LST. In contrast, in other seasons, the feature values in BE, particularly BCR and MH, exhibited a more pronounced distribution. SED has the weakest influence on LST in spring, summer, and winter, while LP has the weakest effect on LST during autumn. This highlights the significant role of vegetation and urbanization in influencing the dynamics of LST.

In terms of the impact of individual indicators, MH, BCR, PD, NDVI, and NTL rank among the top five in terms of influence on LST during spring, autumn, and winter. MH,

BCR, and PD all have an influence intensity greater than 0.1 in these three seasons, while NDVI has an influence intensity greater than 0.1 on LST in spring. The feature points of BCR and PD were predominantly distributed in the positive zone, showing a positive correlation with LST. In contrast, MH was more frequently distributed in the negative zone, exhibiting a strong negative correlation with LST. In summer, the top five indicators influencing LST differ from those in other seasons, ranking as LDI, CNT, NDVI, PD, and MH. Among these, the influence intensity of MH is below 0.1, while the remaining indicators all have an influence intensity greater than 0.1. The feature points of LDI and BCR were primarily distributed in the positive zone, in contrast to MH.

4.3. The Nonlinear Influence of HS Indicators on LST

This study constructed a GBDT model and plotted partial dependence plots (PDPs) to analyze the nonlinear effects of HS indicators on LST. Based on the similarity of the impact trends of HS indicators on LST, the indicators were divided into six groups for discussion. Based on the similarity in the impact trends of HS indicators on LST, the indicators were grouped into six categories, with key indicators from each group discussed in detail.

The first group includes BCR and LDI, as shown in Figure 7A. Building coverage ratio (BCR) and the landscape division index (LDI) exhibit a positive impact trend on LST across all four seasons, with both showing a significant influence on LST within the mid-range of values and tending to stabilize at higher values. In blocks with a high BCR, the heat absorption and retention effects are strong, and the high thermal capacity of building materials leads to a significant increase in LST, which does not vary with seasonal changes. A high landscape division index indicates the isolation of vegetation patches, disrupting the cooling mechanisms of the green space system.

The second group includes ISA and SHDI, as shown in Figure 7B. ISA exhibits a positive impact on LST during spring, summer, and autumn, but in winter, ISA has a slightly negative effect on LST. It is likely that the increase in ISA reduces the cooling effect of ground moisture evaporation, leading to heat retention and a rise in temperature. This effect shows consistency during spring, summer, and autumn, but in winter, the evaporation effect itself is not as prominent. When SHDI is between 0.75 and 1.25, LST decreases significantly, and in winter, SHDI exhibits a notable negative impact on LST after reaching 0.3. This indicates that diversified landscape patches facilitate heat transfer between different thermal patches, reducing LST and improving the urban thermal environment.

The third group includes MH and PD, as shown in Figure 7C. Both MH and PD exhibit a consistent negative impact on LST across all four seasons, and this impact tends to stabilize at higher values. When MH is between 0–20 m, LST decreases significantly, and it decreases slowly between 20–60 m, stabilizing after reaching 60 m. This may be due to the shading effect and wind flow in high-rise building areas, making it difficult for heat to accumulate. When PD is between 50 and 150, LST decreases significantly, indicating that PD density within this range helps in the dispersion and regulation of heat.

The fourth group includes FMD, NTL, NDVI, and CTG, as shown in Figure 8D. The impact trends of FMD, NTL, NDVI, and CTG on LST show seasonal differences. FMD and NTL exhibit a significant negative impact on LST during spring, autumn, and winter. However, summer presents a unique case: FMD has an overall positive impact on LST, while NTL has an overall negative impact. Nevertheless, NTL's influence on LST is weaker when temperatures are below 250 K. NDVI has a negative impact on LST during spring and summer, while its influence on LST during autumn and winter is not significant. In spring, when NDVI ranges from 0.4 to 0.6, LST decreases significantly; in summer, LST decreases significantly when NDVI ranges from 0.25 to 0.6.

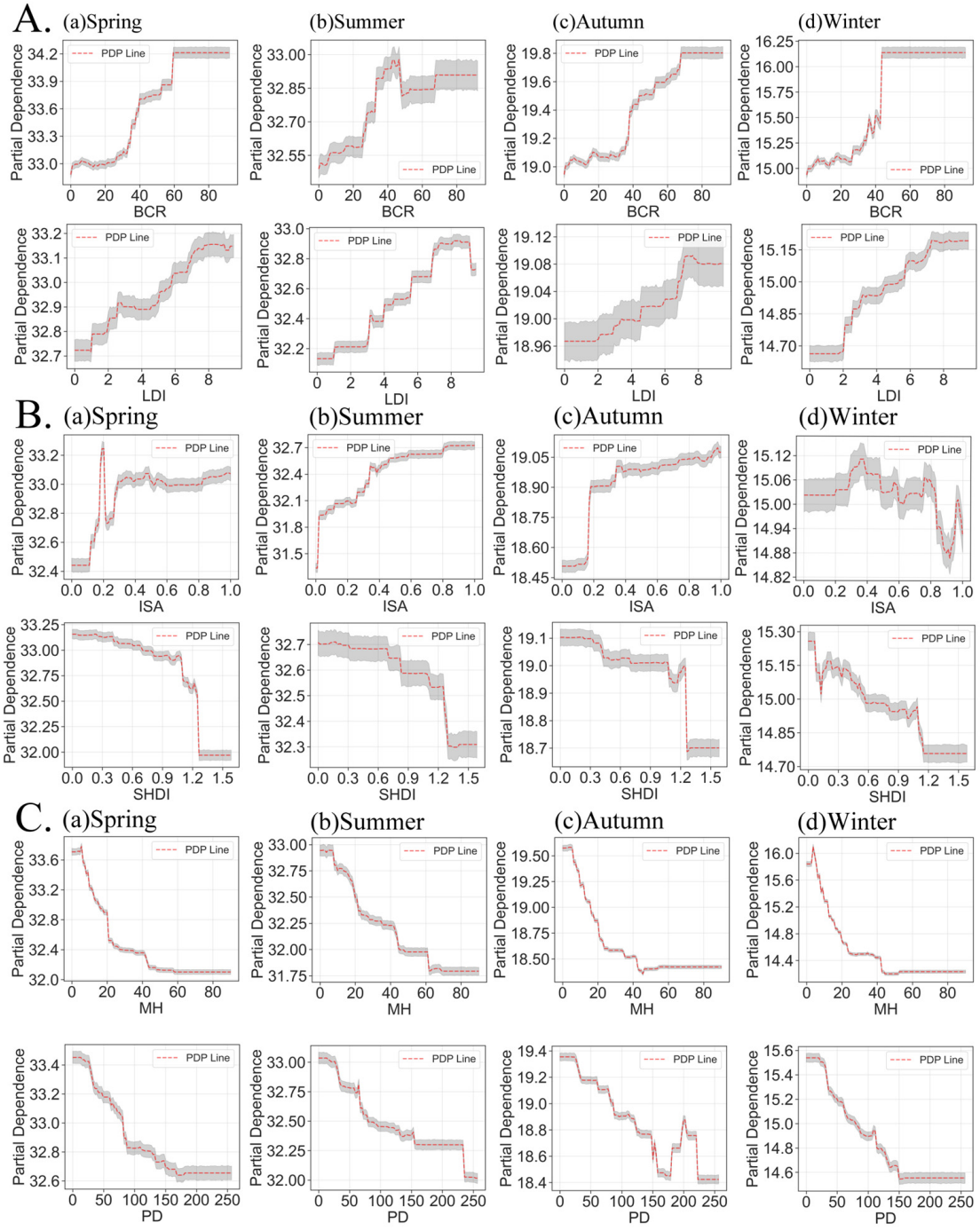

Figure 7. The Partial Dependence Plot (**A**–**C**) of HS indicators on LST.

The fifth group includes CNT and FPD, as shown in Figure 8E. Both CNT and FPD exhibit a clear threshold effect on LST. In summer, CNT remains relatively unchanged when below 80, but once this threshold is exceeded, LST shows a significant upward trend.

The sixth group includes POD and RD, as shown in Figure 8F. In spring, autumn, and winter, POD and RD exhibit a consistent trend, both showing a fluctuating negative impact on LST. However, in summer, POD's impact on LST is not significant, while RD shows a positive impact on LST.

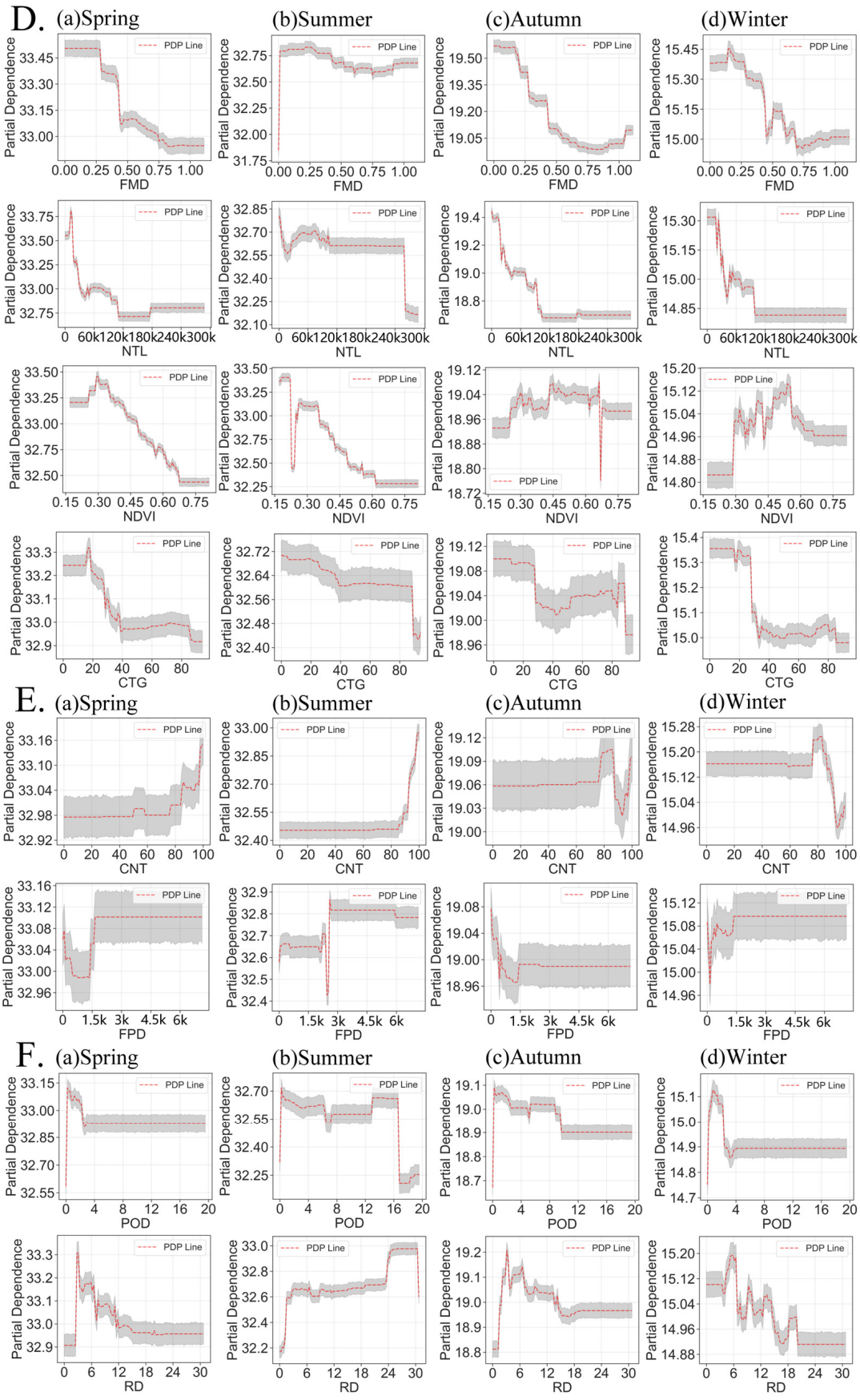

Figure 8. The Partial Dependence Plot (**D**–**F**) of HS indicators on LST.

4.4. The Interactive Effects Between HS Indicators

To further explore the interaction effects of HS indicators on LST, this study selected 16 combinations with the most significant interactions across the four seasons and analyzed the most critical combinations among them. As shown in Figure 6, the x-axis represents one HS indicator, the color bar on the right indicates the other HS indicator with the strongest interaction effect, and the y-axis represents the SHAP interaction value between the two indicators. A SHAP interaction value greater than 0 indicates a positive interaction effect between the two indicators, whereas a negative SHAP interaction value indicates a negative interaction effect. When the SHAP interaction value is less than 0, the larger the absolute value, the stronger the interaction effect, and the greater the reduction in LST.

(1) The Impact of Springtime Interactive Effects on LST

As shown in Figure 9a, As NDVI and MH increase, their interaction effect on LST gradually weakens. When NDVI exceeds 0.5, a negative interaction effect appears between NDVI and MH, and the LST in blocks with high MH gradually decreases. When RD is less than 10, it exhibits a negative interaction effect with high MH values (20–40), contributing to a reduction in LST. When RD is greater than 10, it shows a negative interaction effect with low MH values, also contributing to a reduction in LST.

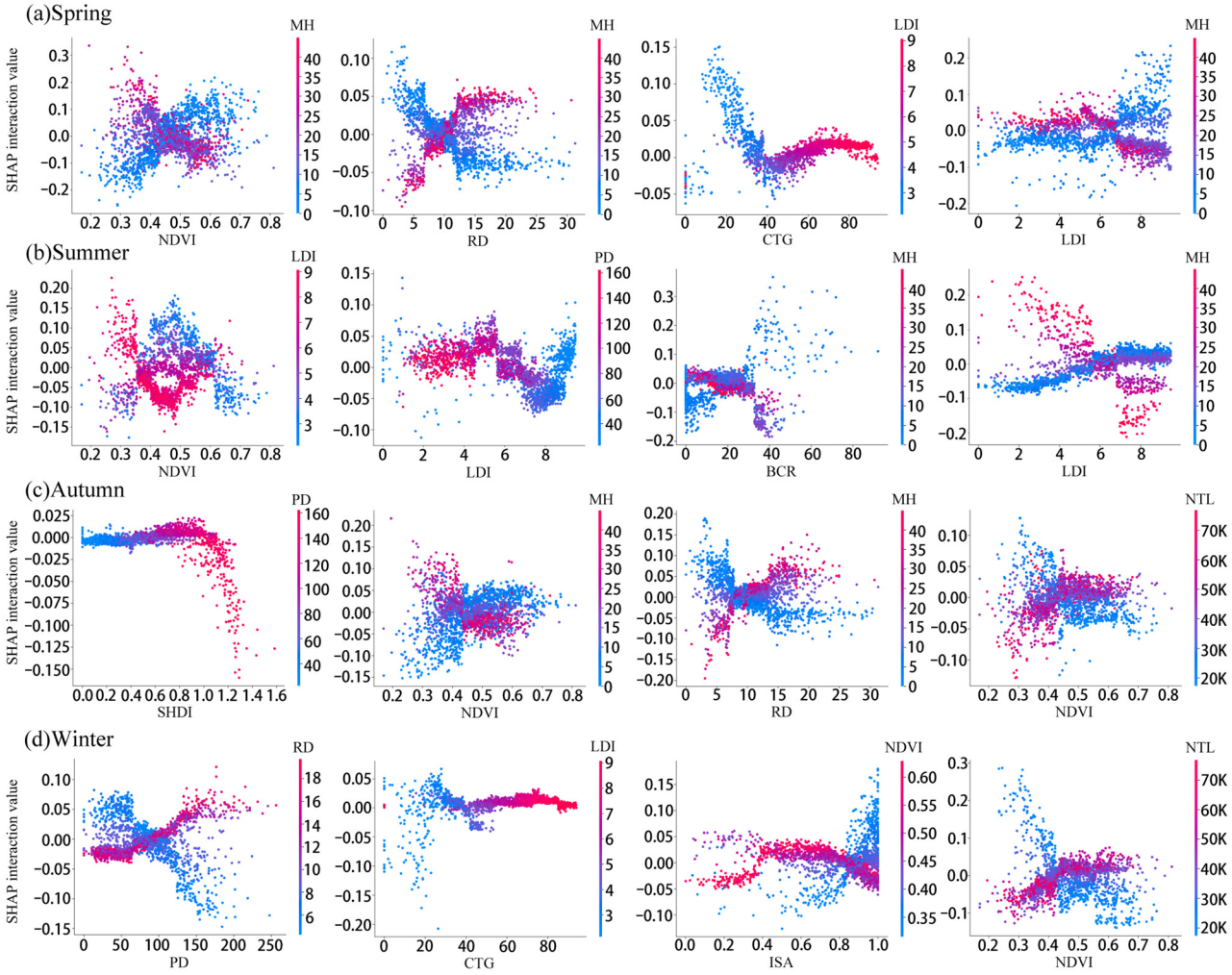

Figure 9. The interactive influence of HS indicators on LST.

(2) The Impact of Summertime Interactive Effects on LST

As shown in Figure 9b, when NDVI is between 0.35 and 0.6, as NDVI increases, it exhibits a negative interaction effect with high LDI values, initially increasing and then

decreasing, which contributes to a reduction in LST. When NDVI exceeds 0.6, it shows a negative interaction effect with low LDI values, also contributing to a reduction in LST. When LDI is less than 6, it shows a negative interaction effect with low MH values; when LDI is greater than 6, it exhibits a negative interaction effect with high MH values. Both scenarios contribute to a reduction in LST.

(3) The Impact of Autumn time Interactive Effects on LST

As shown in Figure 9c, when RD is less than 8, it exhibits a negative interaction effect with high MH values; when RD is greater than 8, it shows a negative interaction effect with low MH values. Both scenarios contribute to a reduction in LST. The interaction effect of NDVI and NTL on LST follows a similar trend as the interaction between RD and MH. When NDVI is less than 0.45, it exhibits a negative interaction effect with high NTL values; when NDVI is greater than 0.45, it shows a negative interaction effect with low NTL values. Both scenarios contribute to a reduction in LST.

(4) The Impact of Wintertime Interactive Effects on LST

As shown in Figure 9d, when PD is less than 90, it exhibits a negative interaction effect with high RD values; when PD is greater than 90, it shows a negative interaction effect with low RD values. Both scenarios contribute to a reduction in LST. The interaction effect between NDVI and NTL on LST mainly results in a strong negative influence. When NDVI is less than 0.4, it exhibits a negative interaction effect with high NTL; when NDVI is greater than 0.4, it shows a negative interaction effect with low NTL. Both scenarios contribute to a reduction in LST.

5. Discussion

5.1. Investigating the Mechanisms of HS's Impact on Seasonal Variations in LST

There is limited research that comprehensively considers the seasonal impact of HS on LST from the three aspects of socio-economic development (SED), built environment (BE), and landscape pattern (LP). This study systematically compares the nonlinear effects of 14 HS indicators on LST across different seasons. Similar to existing nonlinear studies on LST variations, the findings of this study also show that the impact of HS indicators on LST is not a simple monotonic positive or negative correlation [58]. Instead, LST exhibits nonlinear changes with variations in HS indicators, and certain indicators show significant seasonal differences in their impact on LST. The study results show that the building coverage ratio (BCR) within BE elements has a significant impact on LST across all seasons, which aligns with the main conclusions of the previous research [13,14,59]. The likely reason is the heat retention effect in high-density building areas. The findings on NDVI reveal the crucial role of green spaces in regulating LST [60,61]. Urban greening is more effective in reducing LST during spring and summer compared to autumn and winter, which is consistent with the previous research results [13,62]. This may be due to the reduced influence of vegetation during the autumn and winter seasons. ISA has a significant impact on LST, but its influence on LST during winter is less pronounced compared to other seasons, a detail not mentioned in previous studies. This may be due to the high intensity of urban development, which makes city centers more prone to forming localized SUHI effects. Increasing the overall heterogeneity and patchiness of the landscape promotes heat transfer between different thermal patches, thereby reducing LST. The results for patch density (PD) show that a higher number of dense patches contributes to heat dispersion and regulation, which differs from the findings of previous studies using linear regression methods [40]. The results for LDI and CTG indicate that the level of patch connectivity has a significant negative impact on LST. This is likely because highly connected urban landscape patterns help mitigate UHI by establishing urban cool islands and reducing

heat sources [16,25]. This study found that the influence of SED factors on LST varies with the seasons and can affect the spatial distribution of UHI to some extent, similar to the previous research [17]. For example, POD and FMD exhibit significant anomalous trends during the summer. NTL also shows seasonal variations and maintains a negative impact on LST, which differs from the previous studies [18]. This may be due to the stronger spatial heterogeneity of urbanization levels and human activity intensity, as reflected by NTL at the block scale. In city center areas, high-rise buildings cast localized shadow zones during specific periods, mitigating heat accumulation on the ground and building surfaces [63], effectively reducing LST. It can be observed that in such complex urban 3D areas, the satellite-derived imagery data represent a modulated composite surface radiation temperature influenced by geometric morphology. Essentially, this composite temperature serves as an integrated characterization of the thermal properties of urban underlying surfaces, the shading/heat storage effects of three-dimensional structures, and the seasonal energy cycle. To uncover the underlying thermodynamic mechanisms behind the observed data, multi-scale modeling is required.

5.2. Differences in the Impact of HS on LST at the Block Scale

This study used the block scale as the research unit, rather than the traditional 100 m × 100 m small-scale grid. Previous studies have shown that as the research scale changes, the main factors influencing LST also change [18]. Although this choice results in larger unit areas and lower average temperature variations, it enhances the representativeness and realism of this study. It also better captures the heterogeneity and complexity within the urban environment. At the block scale, the interactions between different urban functions and their combined impact on land surface temperature can be more comprehensively reflected. For example, when discussing the relationship between MH and LST, previous studies have simply concluded that MH had a positive impact on LST [64]. However, in some studies that also use the block scale, the relationship between MH and LST shifts from positive to negative as MH values increase, eventually stabilizing in a negative correlation [18]. In the urban morphology of Chengdu's central area, MH consistently shows a significant negative impact on LST. The possible reason is that the sunlit surfaces of towering buildings have a higher albedo, which overshadows the lower albedo of the natural surfaces behind them. The shading effect helps cool the surfaces [65], and the high-albedo building surfaces further reduce heat absorption [18]. Our research findings indicate that at the block scale, studying the impact of HS indicators on LST requires greater attention to the influence of the built environment. In the summer, when the SUHI effect is most pronounced, considering that the combined relative importance of landscape pattern elements exceeds 0.54, special attention should be given to the landscape pattern indices that reflect urban land use patterns. The BE factors dominate in seasons other than summer, primarily due to the significant sensible heat storage capacity of the vast number of buildings in urban centers. This is specifically reflected in the heat accumulation capability of building surfaces. For instance, an increase in BCR leads to a rise in LST. Simultaneously, the localized shadow zones created by high-rise buildings blocking sunlight during specific periods contribute to heat dissipation. However, regardless of whether the impact on LST is positive or negative, BE consistently exhibits its dominant influence. But in summer, LP factors such as LDI play a dominant role, possibly due to the significant heat transfer capacity of specific LPs becoming particularly crucial in periods of intense and concentrated heat. For example, LPs with high connectivity contribute to the formation of urban cooling networks, effectively mitigating the SUHI effect [66].

5.3. Recommendations for Mitigating SUHI Effects

Chengdu's urban expansion, previously driven by economic scale and spatial agglomeration effects [67], has exhibited many common urban issues typical of large metropolitan areas in plains. In the context of both urban expansion and old city renewal, multiple measures need to be adopted to enhance urban thermal resilience [44,68,69]. Focusing on the common dominant factor across seasons, the NDVI, this study analyzed its interactive effects with other HS factors. The results indicate that in spring and autumn, an increase in MH exerts a negative impact on LST in areas with high NDVI. This suggests that in densely built-up areas with high-rise buildings, efforts should be focused on enhancing urban greenery within the blocks [70,71]. In winter, this study of the interaction between NDVI and ISA reveals that in areas with higher ISA, an increase in NDVI enhances its negative impact on LST, demonstrating the significant cooling effect of vegetation on LST. This finding is consistent with the previous research [72]. The study of the interaction between NDVI and NTL shows that in areas with higher NDVI, an increase in NTL enhances the positive impact on LST, further revealing the intrinsic seasonal patterns of LST. These research findings suggest that urban planners can improve the effectiveness of vegetation clusters by adjusting the layout of green spaces in city centers and enhancing vegetation quality through targeted interventions. Chengdu's summer is the most severely impacted by extreme heatwaves. This study shows that in areas with high LDI, an increase in PD significantly enhances the negative impact on LST. This highlights the importance of optimizing the spatial distribution of landscape patches and increasing patch density in urban planning layouts.

5.4. Limitations and Future Prospects

This study has certain limitations. The analysis was conducted solely on Chengdu, and did not account for the influence of meteorological conditions other than cloud cover, anthropogenic activities, or major topographic factors on the results. Due to differences in geographical, climatic, and cultural factors, different cities may exhibit varying thermal environment characteristics. Future research could conduct comparative studies across multiple cities to explore the differences in seasonal SUHI effects between various types of cities, such as coastal and inland cities, and analyze these differences in conjunction with long-term climate change trends. Long-term monitoring and analysis of urban thermal environments could also be conducted to explore the evolving trends of the UHI effect in the context of climate change. This would provide a scientific basis for the sustainable development of cities.

6. Conclusions

This study focuses on the central urban area of Chengdu and adopts the block scale as the research scope. Utilizing the GBDT model and SHAP values, this study explored the nonlinear effects of the human settlements on land surface temperature across different seasons. The main conclusions are as follows:

(1) At the block scale, the primary HS factors influencing land surface temperature (LST) are related to the built environment. The overall impact strength of each factor on LST, in descending order, is as follows: built environment (BE) > landscape pattern (LP) > socio-economic development (SED).

(2) The built environment exerts the strongest influence on LST during spring, autumn, and winter, while landscape pattern has the most significant impact on LST during summer. In terms of the influence strength of individual indicators, MH, BCR, PD, NDVI, and NTL consistently rank among the top five factors influencing LST during spring, autumn, and winter. However, in summer, the top five factors affecting LST

differ from those in other seasons, with LDI, CNT, NDVI, PD, and MH taking the leading positions.

(3) There are seasonal differences in the nonlinear effects of HS indicators on LST. Building coverage ratio (BCR) and the landscape dispersion index (LDI) consistently exhibit a positive impact on LST throughout all seasons. Meanwhile, patch density (PD), the Shannon diversity index (SHDI), the contagion index (CTG), and mean building height (MH) consistently have a negative impact on LST. The impervious surface area (ISA) has a positive impact on LST during spring, summer, and autumn. The normalized difference vegetation index (NDVI) exerts a negative impact on LST during spring and summer. Nighttime light (NTL) and functional mixing degree (FMD) show a negative impact on LST during spring, autumn, and winter. ISA in winter, FMD and NTL in summer, and NDVI during both autumn and winter show no significant impact on LST. As population density (POD) and road network density (RD) increase, their impact on LST shifts from positive to negative during spring, autumn, and winter. In summer, when RD is below 30 km/km^2, it has a positive effect on LST. Connectivity (CNT) and functional density (FPD) exhibit significant threshold effects on LST. Once the threshold is exceeded, LST remains unchanged despite further variations in CNT and FPD.

(4) The interactions between NDVI, LDI, RD, BCR, and MH; NDVI, CTG, and LDI; LDI, SHDI, and PD; NDVI and NTL; ISA and NDVI; as well as PD and RD, exhibit significant effects. The pairwise combinations of these indicators can effectively reduce LST, showing great potential for improving the urban thermal environment. The interaction effects between NDVI and MH, LDI, and NTL are all significant, demonstrating the effective role of coordinated urban green space management in improving the urban thermal environment. This demonstrates that high-rise buildings combined with diversified and well-connected green design can effectively reduce land surface temperature and improve the urban thermal environment. It also indicates that under the influence of intensive human activities in urbanization, a higher-density road network and landscape greening can significantly reduce LST, possibly due to the landscape pattern they create, which is more conducive to heat release.

These findings reveal the complex interactive mechanisms between human settlements variables and LST. By examining the built environment, socio-economic factors, and landscape structure, this study provides strategic recommendations for block-scale cross-seasonal differentiated urban planning. The results offer quantitative and differentiated guidance for policymakers and urban planners committed to improving the urban thermal environment and promoting sustainable urban development.

Author Contributions: Conceptualization, M.Z. and E.W.; methodology, M.Z., Y.M. and T.H.; software, M.Z. and T.H.; validation, M.Z. and M.L.; formal analysis, M.Z. and F.S.; investigation, Y.M. and J.Y.; resources, Y.M. and T.H.; data curation, M.Z.; writing—original draft preparation, M.Z. and T.H.; writing—review and editing, M.Z. and E.W.; visualization, M.Z.; supervision, E.W.; project administration, E.W.; funding acquisition, E.W. All authors have read and agreed to the published version of the manuscript.

Funding: This research were funded by Basic Scientific Research Foundation of the Educational Department of Liaoning Province (No. JYTMS20230627) and the Opening Fund of Liaoning Key Laboratory of Urban and Architectural Digital Technology (No. UADT2024A02).

Data Availability Statement: The data that support the findings of this study are available from the corresponding author, Enxu Wang*, upon reasonable request.

Acknowledgments: We are grateful to our mentor, Lecturer Ji Xian, for his technical guidance and valuable insights on the research methodology. His expertise and meticulous suggestions have

significantly enhanced the scientific rigor of this study and contributed to the overall quality of this manuscript.

Conflicts of Interest: The authors declare no conflicts of interest.

Abbreviations

The following abbreviations are used in this study:

LST	Land surface temperature
UHI	Urban heat island
SUHI	Surface urban heat island
GBDT	Gradient Boosting Decision Tree
SHAP	SHapley Additive exPlanations
HS	Human settlements
SED	Socio-economic development
BE	Built environment
LP	Landscape pattern

References

1. Kim, S.W.; Brown, R.D. Urban heat island (UHI) variations within a city boundary: A systematic literature review. *Urban Clim.* **2019**, *28*, 100464.
2. Chen, M.; Liu, W.; Tao, X. Evolution and assessment on China's urbanization 1960–2010: Under-urbanization or over-urbanization? *Habitat Int.* **2013**, *38*, 25–33. [CrossRef]
3. Berger, C.; Rosentreter, J.; Voltersen, M.; Baumgart, C.; Schmullius, C.; Hese, S. Spatio-temporal analysis of the relationship between 2D/3D urban site characteristics and land surface temperature. *Remote Sens. Environ.* **2017**, *193*, 225–243.
4. Cai, Z.; Han, G.; Chen, M. Do water bodies play an important role in the relationship between urban form and land surface temperature? *Sustain. Cities Soc.* **2018**, *39*, 487–498.
5. Connors, J.P.; Galletti, C.S.; Chow, W.T.L. Landscape configuration and urban heat island effects: Assessing the relationship between landscape characteristics and land surface temperature in Phoenix, Arizona. *Landsc. Ecol.* **2013**, *28*, 271–283.
6. Kumar, A.; Mukherjee, M.; Goswami, A. Inter-seasonal characterization and correlation of Surface Urban Heat Island (SUHI) and Canopy Urban Heat Island (CUHI) in the urbanized environment of Delhi. *Sustain. Cities Soc.* **2022**, *76*, 103668.
7. Bechtel, B.; Demuzere, M.; Mills, G.; Zhan, W.; Sismanidis, P.; Small, C.; Voogt, J. SUHI analysis using local climate zones—A comparison of 50 cities. *Urban Clim.* **2019**, *28*, 100463. [CrossRef]
8. Hidalgo-García, D.; Arco-Díaz, J. Modeling the surface urban Heat Island (SUHI) to study of its relationship with variations in the thermal field and with the indices of land use in the metropolitan area of Granada (Spain). *Sustain. Cities Soc.* **2022**, *87*, 104166.
9. Voogt, J.A.; Oke, T.R. Thermal remote sensing of urban climates. *Remote Sens. Environ.* **2003**, *86*, 370–384.
10. Bansal, P.; Quan, S.J. Examining temporally varying nonlinear effects of urban form on urban heat island using explainable machine learning: A case of Seoul. *Build. Environ.* **2024**, *247*, 110957.
11. Lin, J.; Qiu, S.; Tan, X.; Zhuang, Y. Measuring the relationship between morphological spatial pattern of green space and urban heat island using machine learning methods. *Build. Environ.* **2023**, *108*, 105482.
12. Lin, J.; Wei, K.; Guan, Z. Exploring the connection between morphological characteristic of built-up areas and surface heat islands based on MSPA. *Urban Clim.* **2024**, *56*, 102046.
13. Zhang, Q.; Xu, D.; Zhou, D.; Yang, Y.; Rogora, A. Associations between urban thermal environment and physical indicators based on meteorological data in Foshan City. *Sustain. Cities Soc.* **2020**, *60*, 102288.
14. Xu, Y.; Yang, J.; Zheng, Y.; Li, W. Impacts of two-dimensional and three-dimensional urban morphology on urban thermal environments in high-density cities: A case study of Hong Kong. *Build. Environ.* **2024**, *252*, 111249.
15. Tanoori, G.; Soltani, A.; Modiri, A. Machine Learning for Urban Heat Island (UHI) Analysis: Predicting Land Surface Temperature (LST) in Urban Environments. *Urban Clim.* **2024**, *112*, 104748.
16. Gao, J.; Gong, J.; Yang, J.; Li, J.; Li, S. Measuring Spatial Connectivity between patches of the heat source and sink (SCSS): A new index to quantify the heterogeneity impacts of landscape patterns on land surface temperature. *Landsc. Urban Plan.* **2022**, *217*, 104260.
17. Xi, Y.; Wang, S.; Zou, Y.; Zhou, X.; Zhang, Y. Seasonal surface urban heat island analysis based on local climate zones. *Ecol. Indic.* **2024**, *159*, 111669.
18. Zhang, Z.; Luan, W.; Yang, J.; Guo, A.; Su, M.; Tian, C. The influences of 2D/3D urban morphology on land surface temperature at the block scale in Chinese megacities. *Urban Clim.* **2023**, *49*, 101553.

19. Cao, X. The changes in remoted land surface temperature (LST) triggered by natural and socioeconomic factors in typical Chinese cities. *Sustain. Cities Soc.* **2025**, *118*, 104166.
20. Wang, Z. Revealing the impact of urban spatial morphology on land surface temperature in plain and plateau cities using explainable machine learning. *Sustain. Cities Soc.* **2024**, *118*, 106040.
21. An, Z.; Ming, Y.; Liu, Y.; Zhang, G. Investigating 2D/3D factors influencing surface urban heat islands in mountainous cities using explainable machine learning. *Sustain. Cities Soc.* **2024**, *107*, 104845. [CrossRef]
22. Yu, J.; Hu, Q.; Li, J. Combining visual intelligence and social-physical urban features facilitates fine-scale seasonality characterization of urban thermal environments. *Sustain. Cities Soc.* **2024**, *107*, 104846. [CrossRef]
23. Liu, Y. Exploring the seasonal effects of urban morphology on land surface temperature in urban functional zones. *Sustain. Cities Soc.* **2024**, *107*, 104847. [CrossRef]
24. Yang, C.; Kui, T.; Zhou, W.; Fan, J.; Pan, L.; Wu, W.; Liu, M. Impact of refined 2D/3D urban morphology on hourly air temperature across different spatial scales in a snow climate city. *Urban Clim.* **2023**, *47*, 101404. [CrossRef]
25. Liu, F.; Liu, J.; Zhang, Y.; Hong, S.; Fu, W.; Wang, M.; Dong, J. Construction of a cold island network for the urban heat island effect mitigation. *Sci. Total Environ.* **2024**, *915*, 169950. [CrossRef]
26. Liang, G.; Xu, Z.; Wang, X.; Li, Y.; Li, X.; Zhang, Y.; Wang, J.; Li, J.; Wang, S.; Wang, Y. A multi-species approach for protected areas ecological network construction based on landscape connectivity. *Glob. Ecol. Conserv.* **2023**, *46*, e02569. [CrossRef]
27. Peng, J.; Jia, J.; Liu, Y.; Li, H.; Wu, J. Seasonal contrast of the dominant factors for spatial distribution of land surface temperature in urban areas. *Remote Sens. Environ.* **2018**, *215*, 255–267. [CrossRef]
28. Chen, G.; Li, Y.; Wang, X.; Zhang, Y.; Liu, Z. Assessing the synergies between heat waves and urban heat islands of different local climate zones in Guangzhou, China. *Build. Environ.* **2023**, *240*, 110434.
29. Yang, K.; Tao, F.; Wang, C.-L.; Wang, Z.-L.; Han, Q.-L.; Zhou, T. An optimization method for surface urban heat island footprint extraction based on anisotropy assumption. *Urban Clim.* **2023**, *49*, 101532.
30. Budhiraja, B.; Gawuc, L.; Agrawal, G. Seasonality of surface urban heat island in Delhi city region measured by local climate zones and conventional indicators. *IEEE J. Sel. Top. Appl. Earth Obs. Rem. Sens.* **2019**, *12*, 5223–5232.
31. Cao, Q.; Huang, H.; Hong, Y.; Huang, X.; Wang, S.; Wang, L.; Wang, L. Modeling intra-urban differences in thermal environments and heat stress based on local climate zones in central Wuhan. *Build. Environ.* **2022**, *225*, 109625. [CrossRef]
32. Ezimand, K.; Chahardoli, M.; Azadbakht, M.; Matkan, A. Spatiotemporal analysis of land surface temperature using multi-temporal and multi-sensor image fusion techniques. *Cities Soc.* **2021**, *64*, 102508. [CrossRef]
33. Yang, J.; Jin, S.; Xiao, X.; Jin, C.; Xia, J.; Li, X.; Wang, S. The footprint of urban heat island effect in 302 Chinese cities: Temporal trends and associated factors. *Sci. Total Environ.* **2019**, *671*, 1036–1046. [CrossRef] [PubMed]
34. Lu, Y.; Yue, W.; Liu, Y.; Huang, Y. Investigating the spatiotemporal non-stationary relationships between urban spatial form and land surface temperature: A case study of Wuhan, China. *Sustain. Cities Soc.* **2021**, *72*, 103070. [CrossRef]
35. Yelixiati, H.; Tong, L.; Luo, S.; Chen, Z. Spatiotemporal heterogeneity of the relationship between urban morphology and land surface temperature at a block scale. *Sustain. Cities Soc.* **2024**, *113*, 105711. [CrossRef]
36. Yao, L.; Li, T.; Xu, M.; Xu, Y. How the landscape features of urban green space impact seasonal land surface temperatures at a city-block-scale: An urban heat island study in Beijing, China. *Urban Forestry Urban Green.* **2020**, *52*, 126704. [CrossRef]
37. Deilami, K.; Kamruzzaman, M.; Liu, Y. Urban heat island effect: A systematic review of spatio-temporal factors, data, methods, and mitigation measures. *Int. J. Appl. Earth Obs. Geoinf.* **2018**, *67*, 30–42. [CrossRef]
38. Geng, S.; Yang, L.; Sun, Z.; Wang, Z.; Qian, J.; Jiang, C.; Wen, M. Spatiotemporal patterns and driving forces of remotely sensed urban agglomeration heat islands in South China. *Sci. Total Environ.* **2021**, *800*, 149499. [CrossRef]
39. Gorelick, N.; Hancher, M.; Dixon, M.; Ilyushchenko, S.; Thau, D.; Moore, R. Google earth engine: Planetary-scale geospatial analysis for everyone. *Remote Sens. Environ.* **2017**, *202*, 18–27. [CrossRef]
40. Yang, C.; Zhu, W.; Sun, J.; Xu, X.; Wang, R.; Lu, Y.; Zhang, S.; Zhou, W. Assessing the effects of 2D/3D urban morphology on the 3D urban thermal environment by using multi-source remote sensing data and UAV measurements: A case study of the snow-climate city of Changchun, China. *J. Clean. Prod.* **2021**, *321*, 128956. [CrossRef]
41. Naserikia, M.; Hart, M.A.; Nazarian, N.; Bechtel, B.; Lipson, M.; Nice, K.A. Land surface and air temperature dynamics: The role of urban form and seasonality. *Sci. Total Environ.* **2023**, *905*, 167306. [PubMed]
42. Liu, Y.; An, Z.; Ming, Y. Simulating influences of land use/land cover composition and configuration on urban heat island using machine learning. *Sustain. Cities Soc.* **2024**, *108*, 105482.
43. Yu, S.; Chen, Z.; Chen, Z.; Wu, B.; Zhao, F. Exploring the relationship between 2D/3D landscape pattern and land surface temperature based on explainable eXtreme Gradient Boosting tree: A case study of Shanghai, China. *Sci. Total Environ.* **2020**, *725*, 138229. [PubMed]
44. Liu, Q.; Wang, J.; Bai, B. Unveiling nonlinear effects of built environment attributes on urban heat resilience using interpretable machine learning. *Urban Clim.* **2024**, *56*, 102046.

45. Lan, H.F.; Hou, H.C.; Gou, Z.H. A machine learning-led investigation to understand individual differences and the human-environment interactive effect on classroom thermal comfort. *Build. Environ.* **2023**, *236*, 110956.
46. Zhu, S. Assessing the impact of adjacent urban morphology on street temperature: A multisource analysis using random forest and SHAP. *Urban Clim.* **2024**, *57*, 101982.
47. Li, Y.; Li, Y.; Zhang, Z. Spatiotemporal variations and influencing factors of heatwaves in Chengdu, China. *Atmos. Res.* **2023**, *280*, 106394.
48. Cheng, Z.; Yang, X.; Sun, C.; Xu, Y. The trend of summer urban heat island effect and its relationship with urban development in Chengdu. *Sustain. Cities Soc.* **2022**, *76*, 103457.
49. Chen, Y.; Luo, B.; Xie, S.D. Characteristics of the long-range transport dust events in Chengdu, Southwest China. *Atmos. Res.* **2015**, *122*, 713–722.
50. Zong, H.; Liu, Y.; Wang, Q.; Liu, M.L.; Chen, H. Usage patterns and comfort of gardens: A seasonal survey of internal garden microclimate in the aged care homes of Chengdu City. *Int. J. Biometeorol.* **2019**, *63*, 1181–1192.
51. Peel, M.C.; Finlayson, B.L.; McMahon, T.A. Updated world map of the Köppen-Geiger climate classification. *Hydrol. Earth Syst. Sci.* **2007**, *11*, 1633–1644.
52. Jia, J.; Changjian, N.; Zeyong, H.; Jun, X.; Yuzhu, X. Variation of haze and its relationship with climate change in Chengdu from 1980 to 2010. *Plateau Meteorol.* **2017**, *36*, 517–527.
53. Kumar, L.; Mutanga, O. Google earth engine applications since inception: Usage, trends, and potential. *Remote Sens.* **2018**, *10*, 1509. [CrossRef]
54. Mutanga, O.; Kumar, L. Google earth engine applications. *Remote Sens.* **2019**, *11*, 591. [CrossRef]
55. Friedman, J.H. Greedy function approximation: A gradient boosting machine. *Ann. Stat.* **2001**, *29*, 1189–1232.
56. Lundberg, S. A Unified Approach to Interpreting Model Predictions. *arXiv* **2017**, arXiv:1705.07874.
57. Lundberg, S.M.; Erion, G.G.; Lee, S.-I. Consistent Individualized Feature Attribution for Tree Ensembles. *arXiv* **2018**, arXiv:1802.03888.
58. Li, Z.; Hu, D. Exploring the relationship between the 2D/3D architectural morphology and urban land surface temperature based on a boosted regression tree: A case study of Beijing, China. *Sustain. Cities Soc.* **2022**, *78*, 103392.
59. Liao, W.; Hong, T.; Heo, Y. The effect of spatial heterogeneity in urban morphology on surface urban heat islands. *Energy Build.* **2021**, *244*, 111027.
60. Xi, Z.; Li, C.; Zhou, L.; Yang, H.; Burghardt, R. Built environment influences on urban climate resilience: Evidence from extreme heat events in Macau. *Sci. Total Environ.* **2023**, *859*, 160270.
61. Massaro, E.; Schifanella, R.; Piccardo, M.; Caporaso, L.; Taubenböck, H.; Cescatti, A.; Duveiller, G. Spatially-optimized urban greening for reduction of population exposure to land surface temperature extremes. *Nat. Commun.* **2023**, *14*, 2903. [CrossRef] [PubMed]
62. Hu, Y.; Dai, Z.; Guldmann, J.M. Modeling the impact of 2D/3D urban indicators on the urban heat island over different seasons: A boosted regression tree approach. *J. Environ. Manag.* **2020**, *266*, 110424. [CrossRef] [PubMed]
63. Li, L.; Yu, T.; Zhao, L.; Zhan, Y.; Zheng, F.; Zhang, Y.; Mumtaz, F.; Wang, C. Characteristics and trend analysis of the relationship between land surface temperature and nighttime light intensity levels over China. *Infrared Phys. Technol.* **2019**, *97*, 381–390. [CrossRef]
64. Guo, G.; Zhou, X.; Wu, Z.; Xiao, R.; Chen, Y. Characterizing the impact of urban morphology heterogeneity on land surface temperature in Guangzhou, China. *Environ. Modell. Softw.* **2016**, *84*, 427–439. [CrossRef]
65. Li, J.X.; Song, C.H.; Cao, L.; Zhu, F.G.; Meng, X.L.; Wu, J.G.; Gao, F. Impacts of landscape structure on surface urban heat islands: A case study of Shanghai, China. *Remote Sens. Environ.* **2011**, *115*, 3249–3263. [CrossRef]
66. Qian, W.; Li, X. A cold island connectivity and network perspective to mitigate the urban heat island effect. *Sustain. Cities Soc.* **2023**, *94*, 104525. [CrossRef]
67. Huang, D.Q.; Liu, Z.; Zhao, X.S. Monocentric or Polycentric? The Urban Spatial Structure of Employment in Beijing. *Sustainability* **2015**, *7*, 11632–11656. [CrossRef]
68. Yang, J.; Wang, Y. Optimizing local climate zones to mitigate urban heat island effect in human settlements. *J. Clean. Prod.* **2020**, *275*, 123767. [CrossRef]
69. Luo, X.; Yang, J.; Sun, W.; He, B. Suitability of human settlements in mountainous areas from the perspective of ventilation: A case study of the main urban area of Chongqing. *Sustain. Cities Soc.* **2025**, *118*, 104166. [CrossRef]
70. Hailu, G. Seasonal solar thermal energy storage. In *Thermal Energy Battery with Nano-Enhanced PCM*; IntechOpen: London, UK, 2018.

71. Kim, J.; Lee, S.Y.; Kang, J. Temperature reduction effects of rooftop garden arrangements: A case study of Seoul National University. *Sustainability* **2020**, *12*, 6032. [CrossRef]
72. Cui, F.; Hamdi, R.; Yuan, X.; He, H.; Yang, T.; Kuang, W.; Termonia, P.; De Maeyer, P. Quantifying the response of surface urban heat island to urban greening in global north megacities. *Sci. Total Environ.* **2021**, *801*, 149553. [PubMed]

Disclaimer/Publisher's Note: The statements, opinions and data contained in all publications are solely those of the individual author(s) and contributor(s) and not of MDPI and/or the editor(s). MDPI and/or the editor(s) disclaim responsibility for any injury to people or property resulting from any ideas, methods, instructions or products referred to in the content.